scientific reports

Check for updates

OPEN

A novel liposomal hydrogel loaded with deer blood peptides prevents UVB-induced skin photoaging

Han Bao[1], Ming Zhu[1,3], Yizhuo Xie[1,3], Na Yang[2], Shanshan Wang[1], Kejia Chen[1], Hongzhu Chen[1], Jingwen Dai[1], Zhiping Li[2], Liangping Yu[2]✉ & Jin Pei[1]✉

Ultraviolet (UV) irradiation is a major global contributor to skin damage. To identify novel protective agents, this study evaluated the photoprotective effects of deer blood peptides (DBP) and developed a DBP-based delivery system to prevent UV-induced skin photoaging. DBP was extracted from deer blood via enzyme hydrolysis. In vitro cytotoxicity and cell apoptosis assays confirmed the safety of DBP, while radical scavenging assays and measurements of intracellular reactive oxygen species (ROS) demonstrated its strong antioxidant capacity. Owing to its nutrient-rich composition, potent antioxidant activity, and ability to promote cell proliferation, DBP shows great promise for photoaging therapy. Compared with the free DBP and liposomal DBP (DBP-Lip), the optimized liposome-hydrogel formulation (DBP-Lip-Gel) exhibited superior antioxidant capacity, enhanced skin permeability, and improved stability. In vivo, pretreatment with DBP-Lip-Gel resulted in smoother skin, with histopathological analysis showing a marked reduction in epidermal thickening. Further biochemical assessments revealed that DBP increased glutathione and superoxide dismutase activity while attenuating the UVB-induced elevation of ROS, malondialdehyde, interleukin-1, interleukin-6, and tumour necrosis factor-α. Mechanistic investigations also identified key signaling pathways underlying its photoprotective effects. In conclusion, DBP-Lip-Gel effectively alleviates UVB-induced skin photoaging, underscoring its potential for medical and dermatological applications.

Keywords Antioxidant, Deer blood peptides, Liposome-hydrogel, Nano-formulation, Photoaging, Photoprotective

Abbreviations

ACE	Angiotensin-converting enzyme
CAT	Catalase
Chol	Cholesterol
EVG	Elastic Verhoeff-Van Gieson
DB	Deer blood proteins
DBP	Deer blood peptides
DBP-Lip	DBP liposome
DBP-Lip-Gel	DBP liposome-hydrogel
DL	Drug loading capacity
DLS	Dynamic light scattering
EE	Encapsulation efficiency
ELISA	Enzyme-linked immunosorbent assay
EPC	Egg phosphatidylcholine
GSH-Px	Glutathione peroxidase
HE	Haematoxylin and eosin
IL-1	Interleukin-1
IL-6	Interleukin-6
L929	Mouse fibroblast cells
MAPK	Mitogen-activated protein kinases

[1]Department of Biopharmacy, School of Pharmaceutical Sciences, Jilin University, 1163 Xinmin Street, ChangChun 130021, Jilin Province, People's Republic of China. [2]Department of Clinical Pharmacy, The First Hospital of Jilin University, 1 Xinmin Street, Changchun 130061, Jilin Province, People's Republic of China. [3]Ming Zhu and Yizhuo Xie contributed equally to this work. ✉email: liangpingyu@jlu.edu.cn; peijin@jlu.edu.cn

MDA	Malondialdehyde
PDI	Polydispersity index
ROS	Reactive oxygen species
SOD	Superoxide dismutase
TEM	Transmission electron microscopy
TNF-α	Tumour necrosis factor-α
UVB	Ultraviolet B

Human skin serves as the body's most superficial organ, acting as a crucial barrier against external physical and chemical stimuli[1]. Traditionally, skincare research has concentrated on either therapeutic or cosmetic effects, with a particular emphasis on skin aging[2]. Skin aging is influenced by both internal and external factors. Intrinsic factors include chronological processes such as aging and hormonal changes[3], while extrinsic factors encompass environmental influences such as ultraviolet (UV) radiation exposure and contact with xenobiotics.

Photoaging is primarily caused by UV radiation categorized into UVA (320–400 nm), UVB (280–320 nm), and UVC (200–280 nm) radiation[4]. UVC radiation is absorbed by the stratosphere, whereas UVA and UVB are the main contributors to cutaneous tissue damage[5]. UVB irradiation commonly induces oxidative stress, DNA damage, and inflammation[6], leading to various skin issues such as loss of elasticity, laxity, roughness, thickness, deep wrinkles, and irregular pigmentation, as well as severe conditions like skin cancer[1]. The detrimental effects of UVB are largely attributed to reactive oxygen species (ROS), which are implicated in various diseases, including cancers, cardiovascular diseases, and melanoma[7–10]. Additionally, ROS promotes the production of pro-inflammatory cytokines such as interleukin-1 (IL-1), interleukin-6 (IL-6), and tumour necrosis factor-α (TNF-α), which are directly linked to the activation of the mitogen-activated protein kinases (MAPK) signaling pathway[11–13]. MAPK signaling increases the expression of matrix metalloproteinases (MMPs), which promote collagen degradation and reduce the tensile strength of the dermis. Therefore, an antioxidant substance with strong ROS scavenging capabilities represents a potential candidate for treating UVB-induced skin damage or photoaging[14].

In recent years, researchers have focused on finding antioxidative substances. Some of these include polyphenols and flavonoids extracted from botanicals, while others are protein hydrolysates, especially those rich in collagen from bone and cartilage extractions[15,16]. However, the biological function of peptides is significantly influenced by their molecular structure and weight[17]. Animal blood is a rich source of proteins and has been widely used as a food ingredient in Asia, Africa, and Europe[18]. Blood hydrolysates have demonstrated antimicrobial, antioxidant, and angiotensin-converting enzyme (ACE)-inhibitory properties[19]. Deer blood, in particular, contains water (80–81% of total weight) and protein (18%), along with various lipids, free fatty acids, sterols, glycolipids, phospholipids, hormones, purines, vitamins, polysaccharides, and beneficial trace elements[20]. Notably, the protein content is rich in 20 amino acids, various enzymes, proteins, and polypeptides, which are considered the most prominent bioactive components of deer blood.

Liposomes have been designed as a novel nanoparticle delivery system capable of encapsulating hydrophilic or hydrophobic drugs within a phospholipid bilayer particle; they have been extensively studied in various anti-tumour therapies[21,22]. Meanwhile, liposomes have also been investigated as carrier systems for topical drug delivery. The *stratum corneum* acts as the primary barrier for transdermal drugs, and studies have shown that liposomes can enhance skin permeability[23,24], suggesting their utility for topical drug delivery. Given that liposomes and skin share similar lipid bilayer membrane structures, liposomes exhibit good biocompatibility with skin. However, liposomes still face practical limitations for topical application. To address these shortcomings, we incorporated hydrogels, which confer advantages such as enhancing liposomal stability, prolonging residence time on the skin surface, reducing the degradation, and ease of application[25,26].

Deer blood peptides (DBP) possess rich nutrients, antioxidant capabilities, and promoting cell proliferation. Also, compared with the peptides in other resource, the content of essential amino acids and hydrophobic amino acids in DBP was significantly higher than that in marine peptides[27]. The antioxidant activity of DBP was also superior to that of marine peptides[28]. These characteristics of DBP could effectively protect skin cell from damages caused by ultraviolet radiation. Moreover, little research has been conducted in the effects of DBP liposome hydrogel on the protective potential against UVB-induced skin photoaging. In this study, DBPs were prepared and characterized. Liposomal-hydrogel delivery system for DBPs (DBP-Lip-Gel) was designed and prepared. With this work, we aim to develop a DBP-loaded topical product to counteract UVB-induced skin aging.

Materials and methods

Chemicals and reagents

Deer blood powder was purchased from Zhonglu Co., Ltd. (Changchun, China). Alcalase was purchased from Yuanye Co., Ltd. Egg yolk lecithin (EPC), cholesterol (Chol), and BCA protein assay kits were purchased from Dalian Meilun Biotechnology Co., Ltd. Polysorbate 80, DAPI, and rhodamine B (RhB) were purchased from Tianjin Guangfu Fine Chemical Research Institute. Cell Counting Kit-8 (CCK8) was purchased from Invigentech, Inc. ROS assay kit was purchased from Yeasen Biotech Co., Ltd. Apoptosis and cell cycle analysis kits were purchased from Elabscience Biotechnology Co., Ltd. Commercial enzyme-linked immunosorbent assay (ELISA) kits for superoxide dismutase (SOD), catalase (CAT), glutathione peroxidase (GSH-Px) malondialdehyde (MDA), reactive oxygen species (ROS), interleukin-1 (IL-1), interleukin-6 (IL-6), and tumour necrosis factor-α (TNF-α) were purchased from Jingmei Biotechnology Co., Ltd. Primary antibodies against Bax, Bcl-2, caspase-3, COL1A1, MMP-3, TGF-β, Smad 2/3, ERK, JNK, P38, p-ERK, p-JNK, p-P38, and GAPDH, as well as secondary antibodies, were purchased from ABclonal Technology Co., Ltd. All of the reagents listed above were analytical or higher grade.

Preparation of DBP

DBP was prepared by the enzymolysis method[29]. Briefly, deer blood powder was dissolved in water thoroughly, followed by sonicating and shaking at room temperature. Subsequently, 5% (w/w) alcalase was added and mixed thoroughly, and then NaOH was added to adjust the pH to 9.0. This mixture was incubated for 4 h at 55 °C, followed by deactivation of enzyme activity in a 95 ℃ water bath for 10 min. Following this, HCl was added to the sample to adjust the pH to 7.0. The sample was then centrifuged at 9,500 rpm for 10 min to separate the supernatant, which contained the DBP. Finally, the DBP solution was lyophilized for subsequent use.

Molecular weight distribution of DBP

Deer blood proteins (DB) and DBP were analyzed by SDS-PAGE electrophoresis[30]. In brief, 30 μg of the DB sample was loaded onto a 10% SDS-PAGE gel, while the DBP sample was loaded onto a 17.5% Tris-tricine-SDS-PAGE gel, followed by electrophoresis. After this, the gels were stained with Coomassie brilliant blue for 2 h, followed by de-staining in 25% (v/v) methanol and 10% (v/v) acetic acid for 4 h until clear bands were observed on the gels. The images were taken using a digital camera.

Determination of amino acid composition and content of DBP

The amino acids composition of DBPs was detected by an automatic analyzer[16].

Briefly, the DBP sample was dissolved in 5 mL of 6 M HCl, thoroughly mixed, and then hydrolyzed at 110 °C for 24 h. After cooling, both the DBP sample and standard samples were loaded into the amino acid analyzer, and the amino acid composition of DBP was determined based on the standard curve. Additionally, the DBP content was quantified using the BCA method.

Measurement of antioxidant activity of DBP

The antioxidative effect of DBPs was determined by evaluating the DPPH free radical scavenging activity and an ABTS free radical scavenging method as follows[31]. In brief, equal volumes (2 mL) of DPPH solution (1.0×10^{-4} mol/L) and DBP solution (1, 2, 5, 10, or 15 mg/mL as final concentrations) were mixed thoroughly and held in the dark at room temperature for 30 min. Subsequently, the absorbance was determined spectrophotometrically at 517 nm.

The DPPH radical scavenging rate was calculated as follows:

$$\text{Scavenging rate } (\%) = [1 - (\text{A1} - \text{A2})/\text{A3}] \times 100\%$$

Where A1 is the absorbance of DPPH in the sample, A2 is the absorbance of anhydrous ethyl alcohol in the sample, and A3 is the absorbance of DPPH in the solvent.

For the ABTS experiment[32], equal volumes of ABTS stock solution (7.0 mmol/L) and potassium peroxodisulphate (2.45 mM) were mixed vigorously and then incubated overnight to generate ABTS·+ radicals at room temperature. The ABTS concentration was adjusted to an absorbance of 0.70 ± 0.02 as measured spectrophotometrically at 734 nm. Equal volumes (2 mL) of ABTS radical solution and samples at different concentrations (0.1, 0.25, 0.5, and 1.0 mg/mL) were mixed and held in the dark at room temperature for 30 min.

The ABTS·+ radical scavenging rate was calculated as follows:

$$\text{Scavenging rate } (\%) = (\text{As} - \text{Ac})/\text{As} \times 100\%$$

Where Ac is the absorbance of ABTS in the sample, and As is the absorbance of ABTS in the solvent.

Preparation of the DBP-Lip and DBP-Lip-Gel

Liposomes were prepared using the thin-film hydration method[33]. Briefly, 118 mg EPC, 20 mg Chol, and 2 μL Polysorbate 80 were dissolved in 15.0 mL chloroform in a round-bottom flask. The chloroform was removed using a rotary evaporator for 30 min, which caused a thin film to form at the bottom of a 37 °C water bath. The lipid film was dried under nitrogen overnight to remove the chloroform residue. Subsequently, the dried lipid film was hydrated with water containing DBP (4 mg/mL) at 37 °C for 2 h, followed by sonication for 10 min in an ice bath. The formulations were then sequentially extruded through 450 nm and 220 nm polycarbonate membranes five times each. Finally, the liposomes (DBP-Lip) were obtained.

The hydrogel was prepared as described previously[34]. Briefly, 60 mg carbomer-980 powder was dissolved in 10 mL water and stirred overnight. The carbomer matrix was mixed with an equal volume of DBP-Lip and stirred to ensure the uniform distribution of the DBP-Lip in the hydrogel. Finally, by adding a solution of triethanolamine until pH 6.5, the final liposome-hydrogel formulation (DBP-Lip-Gel) was obtained.

Characterization of the DBP-Lip and DBP-Lip-Gel

The encapsulation efficiency (EE) and drug loading capacity (DL) of DBP-Lip were determined by BCA assay[35]. In brief, the unencapsulated free DBP was removed by dialysis, and then 0.1 mL DBP liposome solution was added to 1.9 mL 3% (v/v) Triton X-100. The samples were vortexed for 1 min and incubated at 37 °C for 30 min before testing. The EE and DL were calculated using the following formulas:

$$\text{EE } (\%) = (\text{amount of DBP entrapped in liposomes/initial amount of DBP added}) \times 100\%$$

$$\text{DL } (\%) = (\text{amount of DBP entrapped in liposomes/total amount of liposomes}) \times 100\%$$

The main parameters of liposomes considered were average size, size distribution (polydispersity index, PDI), zeta potential, and morphology. Particle size, PDI, and zeta potential of DBP-Lip were determined by dynamic

light scattering (DLS) using a Zetasizer 2000 (nano-ZS 90, Malvern, UK) at 25 °C. The morphology of DBP-Lip was determined by transmission electron microscopy (TEM, H-800, Hitachi, Japan) at 80 kV operating voltage. In brief, the sample was placed on a copper grid covered by carbon film and stained with phosphotungstic acid (3.0%, w/v). The morphology of DBP-Lip-Gel was observed using scanning electron microscopy. In brief, the DBP-Lip-Gel sample was freeze-dried for 48 h prior to observation. The dries sample was mounted on the stub using adhesive carbon tape and sputter-coated with gold-palladium (Au-Pd) under an argon atmosphere. Morphological observation was then conducted using a scanning electron microscope (JSM-IT500A).

In vitro release from different DBP formulations

An in vitro release study was performed in PBS at 37 °C using the dialysis method[36]. Briefly, free DBP, DBP-Lip, and DBP-Lip-Gel was introduced into a dialysis bag (MWCO = 50 kDa) and sealed tightly, respectively. Then, the dialysis bag was placed into a 50.0 mL release medium (PBS) and incubated in an orbital shaker for 48 h at 37 °C. At predetermined time points of 0, 1, 2, 4, 6, 12, 24, and 48 h, samples (0.3 mL) in dialysis bags were collected, and nine times volume of 3% (v/v) Triton X-100 was added for demulsification. The concentration of DBP was determined by BCA assay. The cumulative release rate was calculated according to the following formula:

$$\text{Cumulative release rate } (\%) = (\mathrm{C_0} - \mathrm{C_n})/\mathrm{C_0} \times 100\%$$

In which C_0 represents the DBP concentration at 0 h, and C_n represents the DBP concentration at predetermined time points.

Skin permeation of different DBP formulations

Skin permeation was evaluated using the Franz diffusion cells method[37]. In brief, normal Sprague-Dawley (SD) rats were anesthetized and euthanized. The abdominal hair was removed with a razor and hair removal cream with care to maintain skin integrity. Rat abdominal skin was carefully separated and adherent subcutaneous fat gently removed, and then the treated skin was cleaned with normal saline, placed in a suitable container, and stored at − 20 °C. The percutaneous permeability of DBP formulations were detected by the Franz diffusion cell system. The treated skin of the rats was located between the receiving pool and the diffusion pool. The side of the cuticle was left facing up. The receiving tank was injected with normal saline, and the same concentrations of free DBP, DBP-Lip, and DBP-Lip-Gel were put into the diffusion tank, which was kept at 37 ± 2 °C under moderate agitation. At predetermined time points (1, 2, 4, 6, 8, 10, 12, and 24 h), 0.2 mL was removed from the receiving pool and immediately replaced with the same amount of saline. The DBP content was determined by the BCA method. The cumulative transmittance is calculated using the following formula:

$$Q_n = \frac{C_n V_0 + \sum_{i=1}^{n-1} C_i V_s}{\mathrm{A}}$$

Where Q_n stands for unit cumulative transmittance (μg·cm^{-2}); C_n is the drug concentration at each sampling time point t (μg·mL^{-1}); Ci is the drug concentration (μg·mL^{-1}) before sampling time point; V_0 is the volume of the receiving pool (mL); Vs is the volume of the receiving fluid sampled (mL), and A is the effective permeable area of the diffusion cell (cm^2).

Storage stability of different DBP formulations

The stability of DBP-Lip was measured in ultrapure water at 4 °C and 25 °C. The leakage rates were calculated over 28 h as indicators of stability[38]. At predetermined time points of 0, 1, 2, 7, 14, and 28 h, an aliquot of the sample was pipetted out and free DBP was removed as described above. The remaining DBP content in the liposome was quantified using BCA assay. The concentrations of DBP inside liposomes at different time points were recorded as Cn (n = 0, 1, 2, 7, 14, or 28 h). C0 represents the DBP concentration at 0 h. The drug leakage rate was calculated using the following formula:

$$\text{Leakage rate } (\%) = (1 - \mathrm{Cn}/\mathrm{C0}) \times 100\%$$

To assess the storage stability of DBP-Lip stored at 4 °C. The particle size, PDI and Zeta potential of DBP-Lip was measured at predetermined time points of 1, 2, 7, 14, and 28 day. 0.1 mL sample of DBP-Lip was diluted in ultrapure water with the ratio of 1:100 (v/v) and determined by dynamic light scattering (DLS) using a Zetasizer 2000 (nano-ZS 90, Malvern, UK). To assess long-term storage stability of DBP different formulations[39], the DBP content of DBP solution, DBP-Lip and DBP-Lip-Gel stored at 4 °C for 6 months was determined by BCA assay. At each time point, a 1.0 mL sample of each liposomal formulation was mixed with Triton X-100 for demulsification before testing. A 1.0 mL sample of the hydrogel formulation was mixed with isopropyl alcohol before testing.

Cell culture and UVB irradiation

Mouse fibroblast cells (cell line L929, purchased from Wuhan Procell Life Science & Technology Co., Ltd.) were cultured in minimum essential medium (MEM) with 10% foetal bovine serum (FBS) and 1% penicillin-streptomycin (P/S). The cells were cultured in an incubator at 37 ℃ and with 5% CO_2 humidified air. The cells were counted and seeded in plates with various numbers of wells for different experiments for 24 h[40] and then pre-treated with different concentrations of DBP for 12 h. After that, the culture medium was discarded and replaced with PBS, and cells were placed 9 cm below a lamp for exposure to UVB irradiation (40 mJ/cm^2). The PBS was then replaced with fresh MEM without FPS, the cells were cultured for another 12 h, and then they were collected for further analysis. Control cells were treated similarly, without UVB exposure and DBP treatment.

Cell uptake with different formulations

L929 cells were seeded in 24-well plates at a density of 5.0×10^3 cells/well with MEM containing 10% FBS and 1% penicillin-streptomycin at 37 °C and 5% CO_2. After 24 h of incubation, the cells were treated with free RhB, RhB liposomal formulation (RhB-Lip) and RhB liposomal hydrogel formulation (RhB-Lip-Gel) at a 5.0 μg/mL final Rh B concentration for 3 h. After this, the cells were washed with cold PBS three times and fixed with 4% paraformaldehyde. DAPI was applied for 30 min to stain nuclei. Subsequently, the cells were observed and imaged under a fluorescence microscope (Ts2-FL, Nikon). Quantitative fluorescence results were evaluated using Image Processing and Analysis Java (ImageJ)1.51 (National Institutes of Health, Bethesda, Maryland, USA).

Cytotoxicity of DBP formulations in L929 cells

The cytotoxicity of DBP in L929 cells was evaluated by measuring cell viability after treatment with different concentrations or formulations of DBP. The cells were cultured as described above, and cytotoxicity was measured using CCK8 kits according to the manufacturer's instructions. In brief, the L929 cells (2.0×10^3cells/well) were seeded in flat-bottom 96-wells plates, and, after incubation for 24 h, the medium was replaced with fresh MEM with or without different concentrations or formulations of DBP. The cells were cultured for another 24 h and then the media were replaced with fresh MEM with 10% CCK8 solution and incubated for an extra 2 h before determining absorbances spectrophotometrically at 450 nm. Based on absorbances, the control group was regarded as 100% viable and the percentage viability of various groups was determined as compared to the control.

To determine the viability of UVB-induced cells, L929 cells were seeded in flat-bottom 96-well plates overnight. Then, cells were administrated different concentrations or formulations of DBP for 12 h. Then, the medium was exchanged for PBS. Following exposure to UVB irradiation, the cells were washed once with PBS, incubated for another 12 h, and then assessed with CCK8 kits.

Determination of intracellular ROS levels

L929 cells were seeded in 24-well plates at a density of 5.0×10^3 cells/well. After 24 h of incubation, cells were pre-treated with different concentrations or different formulations of DBP and exposed to UVB radiation. Then, 12 h after incubation, the DCFH-DA was added at a final concentration of 10 μM, and the cells were incubated for 2 h and then washed with PBS three times. Subsequently, the cells were observed and imaged under a fluorescence microscope (Ts2-FL, Nikon). Quantitative fluorescence results were evaluated using ImageJ software.

Cell apoptosis

The cells were cultured under the same conditions as above. After treatment with UVB, a sample with 5×10^5 cells was centrifuged at 300 g for 5 min and washed with PBS once, and then 100 μL Annexin V Binding Buffer was added to resuspend the cells. Annexin V-FITC (2.5 μL) and 7-AAD (2.5 μL, 100 μg/mL) reagents were added, and, following a gentle vortex, the cells were incubated for 20 min. Annexin V Binding Buffer (400 μL) was added and mixed well, and then the cells were analyzed on a BD Accrui™ C6 Plus flow cytometer using the FITC channel for Annexin-V-FITC and the PerCP/Cy5.5 channel for 7-AAD.

UV-induced Photoaging animal model

ICR mice, aged 4 to 6 weeks old and weighing 20 ± 2 g (purchased from Changchun Biotechnology Co., Ltd.), were used in experiments. All mice were reared indoors under a 12-hour light/dark cycle. Animals were housed in standard cages and given free access to food and water. All the anesthesia procedures for the animals in this study were carried out by intraperitoneal injection of sodium pentobarbital.

To establish the UV-induced photoaging model, 60 mice were divided into ten groups randomly (six mice in each group): (1) normal group (Normal), mice were administered PBS without exposure of UVB; (2) model group (Model), mice were administered PBS and exposed to UVB; (3) positive control group (Vc), mice were administered vitamin C and exposed to UVB; (4) free DBP low dose group (DBP-L), mice were administered free DBP (150 mg/kg) and exposed to UVB; (5) free DBP high dose group (DBP-H), mice were administered free DBP (300 mg/kg) and exposed to UVB; (6) liposomal DBP low dose group (DBP-Lip-L), mice were administered DBP liposomal formulation (150 mg/kg) and exposed to UVB; (7) liposomal DBP high dose group (DBP-Lip-H), mice were administered DBP liposomal formulation (300 mg/kg) and exposed to UVB; (8) liposomal-hydrogel DBP low dose group (DBP-Lip-Gel-L), mice were administered DBP liposomal-hydrogel formulation (150 mg/kg) and exposed to UVB; (9) liposomal-hydrogel DBP high dose group (DBP-Lip-Gel-H), mice were administered liposomal-hydrogel formulation (300 mg/kg) and exposed to UVB; (10) negative control group (Blank-Lip-Gel), mice were administered blank liposomal gel formulation and exposed to UVB.

Depilation of the ICR mouse dorsal skin was performed for an area 2 cm × 2 cm, and the different formulations were topically applied. Then, the mice were exposed to UVB irradiation under a UVB lamp (Philips TL 20w/12RS, Philips, Holland; wavelength of 311 nm) placed 9 cm above the cage. Administration of different samples in each group was followed by UVB irradiation three times per week for 9 weeks. The UVB intensity employed in the experiment was calibrated as follows: 1 minimal erythema dose (MED; 60 mJ/cm^2) during the first week, 2 MEDs during the second and third weeks, 3 MEDs during the fourth through sixth weeks, and 4 MEDs during the seventh through ninth weeks. The mice dorsal skins were observed and recorded every week for 9 weeks, and the dorsal skins were taken images using a digital camera. The mice body weight was recorded at the determined time. At the end of the experiments, the mice were euthanized by injection with an overdose of sodium pentobarbital (200 mg/kg i.p.), the blood samples were centrifuged and the supernatant was collected for further use. The dorsal skins were collected to be stored in 10% paraformaldehyde or – 80 °C refrigerator for further use. The main organs of heart, liver, spleen, lungs, and kidneys were collected and weighted for the

determination of the organ coefficient. The mice were randomly assigned in vivo experiment and the sample sizes (n) was described in all the figure legend.

Histological examination

Mouse dorsal skin samples were embedded in paraffin, and then a 5-μm-thick section was cut for histological evaluation. Haematoxylin and eosin (HE), Masson's, and elastic Verhoeff-Van Gieson (EVG) staining were performed. The stained slides were photographed under an optical microscope (Nikon, Tokyo, Japan). Epidermal thickness was measured using Image J software. Lengths of the epidermis were determined from three different locations of each mouse's dorsal skin to calculate an average. The density of collagen fibres and elastic fibres was examined using Masson's trichrome staining at 100× magnification, and the collagen density was quantified using the Image Pro Premier 9.1 program.

ELISA

The photoaging effect caused by ultraviolet irradiation was evaluated by using ELISA kits to detect the expression levels of SOD, CAT, GSH-Px, IL-1, IL-6, TNF-α, ROS, and MDA in serum and dorsal skin tissue, as per the manufacturer's instructions.

Western blot analysis

Mouse dorsal skins were collected, and proteins were extracted for western blot analysis, following the kit manufacturer's instructions. For each 20 mg tissue, 150 μL RIPA buffer with 1% PMSF was added. Samples were homogenized 10 times for 1 min each in an ice bath, following by centrifugation at 12,000 g and 4 ℃ for 10 min. The supernatants were collected and transferred into a new tube. Then, the concentration of protein in each sample was measured using a BCA kit. After uniformization of sample concentrations, 30 μg protein in each sample was loaded onto a 10% SDS-PAGE gel for electrophoresis and then transferred to 0.22-μm PVDF membranes. After blotting with Tris-buffered saline with Polysorbate 20 (TBST) containing 5% (w/v) skim milk for 1 h, the membranes were incubated with primary antibody at a dilution of 1:1000 and 4 ℃ overnight. Subsequently, the membranes were washed three times and a second antibody was added at a dilution of 1:10000 for 2 h at room temperature. The bands were visualized using Tanon Imaging System (Tanon-4600; Tanon Co., Ltd., Shanghai, China). Protein expression levels were quantified using Image J software.

Skin safety studies

For the acute dermal toxicity test of DBP-Lip-Gel, ten SD rats (purchased from Changchun Biotechnology Co., Ltd.) were anesthetized and the hair on their backs was carefully shaved. DBP-Lip-Gel was smeared evenly on the back skin of each rat at a dose of 2000 mg/kg. At 24 h after administration, the residual on the back was removed. The skin of the rats was observed for erythema every day and photographed on days 0, 7, and 14 after treatment.

For multiple skin irritation testing of liposomal hydrogel formulations, six SD rats were anesthetized to remove their dorsal hair. An area of 3.0 cm × 3.0 cm was randomly selected on the left and right sides of the back. The DBP-Lip-Gel was applied on the left side of the back and a blank formula was applied on the right side, both at a dose of 0.1 mg/mL once daily for 14 days. The skin was observed for erythema every day and photographed on days 0, 7, and 14 after administration. The degree of skin irradiation with different dosages was recorded.

For skin sensitization testing, ten healthy female adult guinea pigs (purchased from Changchun Biotechnology Co., Ltd.) were chosen. Their dorsal hair was shaved for a smeared area of 2 cm × 2 cm. For inducive contact testing, 0.2 mL of DBP-Lip-Gel was smeared on the left dorsal skin, followed by 6-hour closed application. The above steps were repeated on days 7 and 14. In the negative control group, blank formula was applied in the same way. For stimulate contact testing, 14 days after the last inducing treatment, 0.2 mL of DBP-Lip-Gel was smeared on the right dorsal skin, followed by 6-hour closed application. At 24 h and 48 h after stimulating contact with DBP-Lip-Gel, the skin reaction on the back of the guinea pigs was observed and scored. Guinea pig skin was photographed on days 0, 7 14, 29, and 30.

Statistical analysis

Statistical significance was determined through an unpaired t-test or one-way ANOVA followed by Tukey's multiple comparison post-hoc test (GraphPad Prism version 8.0). $p < 0.05$ was considered statistically significant.

Results

Molecular weight distribution and amino acid composition of DBP

Molecular distribution is a crucial parameter for characterizing the properties of protein or peptide. First, we examined protein content in the original material. The protein content of deer blood had a molecular distribution similar to that of bovine serum albumin (Fig. 1A), indicating that deer blood was abundant in serum albumin. Furthermore, high antioxidant activity of bioactive peptides is generally indicated by a molecular weight less than 10 KDa[41]. To obtain low molecular weight peptides, the deer blood was hydrolysed with the proteolytic enzyme alcalase at a ratio of 5% (w/w). The molecular weight distribution of DBPs in deer blood hydrolysate showed molecular weights mainly below 7.8 KDa (Fig. 1B). Moreover, we examined the nutrient content of DBP. The content of each amino acid residue was obtained by dividing its content by the total content of all amino acid residues (Fig. 1C). The results indicated that DBP was abundant in various amino acids, especially essential amino acids like alanine and leucine, which comprised 11.68% and 12.08%, respectively, of total amino acid content (Table S1). In addition, hydrophobic amino acids are known to be associated with antioxidative activity[27]. Therefore, we investigated the hydrophobic amino acid content and found it comprised 49.60% of the

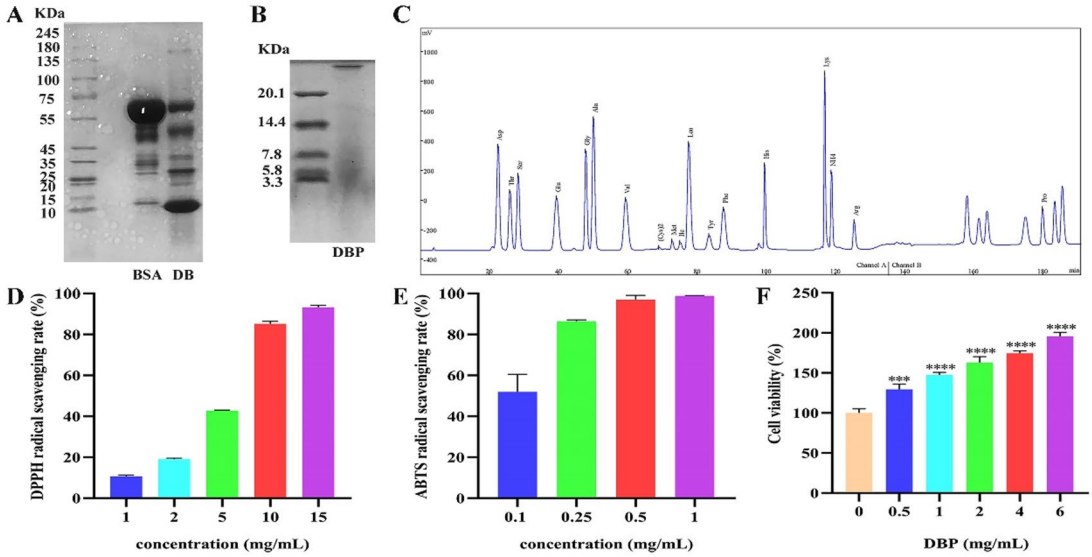

Fig. 1. Characterization of deer blood peptides (DBP). (**A**) The molecular distribution of DB. (**B**) The molecular distribution of DBP from deer blood hydrolysate. (**C**) The retention time of different amino acids contents in DBP. (**D**) The antioxidant capacity of DBP measured by detecting DPPH radical scavenging activity. (**E**) The antioxidant capacity of DBP measured by detecting ABTS radical scavenging activity. (**F**) In vitro cytotoxicity of free DBP with concentration ranging from 0.5 to 6 mg/mL in L929 cells. Data was presented as the mean ± standard deviation; $^{***}p < 0.001$ and $^{****}p < 0.0001$ compared to the non-DBP treatment group, $n = 3$.

total amino acid content, which means DBPs have potential antioxidative properties. These results revealed that DBPs are not only rich in nutrients but also in amino acids suggesting potential antioxidant activity.

Antioxidant activity and cytotoxicity of DBPs

To further characterize the DBP, we detected their antioxidant activity using ABTS and DPPH methods. Results of both methods were read as colour reactions that indicated antioxidant viability. DPPH and ABTS radicals are violet-coloured when transferred into the colourless non-radical solution. We found that the higher the concentration of DBP, the higher the scavenging activity, meaning that high concentrations of DBP displayed strong antioxidant activity (Fig. 1D–E). In addition, the IC_{50} values of scavenging activity were 4.93 mg/mL and 0.10 mg/mL using the DPPH and ABTS methods, respectively. IC_{50} values directly showed the antioxidant activity of DBP, while the lower value showed higher antioxidant activity[42]. These results indicated that the antioxidant activity of DBP was satisfactorily high.

We also evaluated the cytotoxic effects of DBP on L929 cells. Based on the cell viability analysis, the DBP had no cytotoxic effect (Fig. 1F). On the contrary, treatment of L929 cells with DBP up to 6 mg/mL promoted cell viability to 200.0%. This result indicated that DBP can promote the proliferation of L929 cells in a dose-dependent manner, indicating that DBP possesses high nutritional value.

Characterization of DBP formulations

As the primary parameters of liposomes, particle size, zeta potential, and PDI can be used to directly characterize liposomes. The liposomes in our study were prepared using the thin-film hydration method. As shown in Fig. 2A; Table 1, the particle size of DBP-Lip was 111.4 ± 2.8 nm. The smaller particle size will be more likely to increase the skin permeation[43]. Furthermore, the PDI of DBP-Lip was less than 0.3, which indicated that DBP-Lip had a uniform distribution. Moreover, the zeta potential of DBP-Lip was approximately − 30 mV. The zeta potential indicated the stability of liposomes based on surface charge: the higher the absolute value of the zeta potential, the higher the stability of liposomes[44]. The results indicated that the prepared liposomes had impressive stability. The morphology of DBP-Lip was detected by TEM. As shown in Fig. 2B–C, the prepared liposomes exhibited a spherical shape with uniform particle size in a homogeneous dispersion state, consistent with the results determined by DLS.

In addition, the morphology of DBP-Lip-Gel was assessed by scanning electron microscopy. As shown in Fig. 2D–E, the hydrogel base was observed to provide a porous network structure that allowed uniformly distribution of the spherical liposomes.

In vitro release and skin permeation of DBP formulations

An in vitro release study was performed in PBS at 37 ℃, as shown in Fig. 2F. Free DBP exhibited fast release behaviour and showed complete release within 10 h. In comparison, DBP-Lip and DBP-Lip-Gel showed prolonged release behaviour without a burst, indicating that the liposomal formulation slowed the release of DBPs.

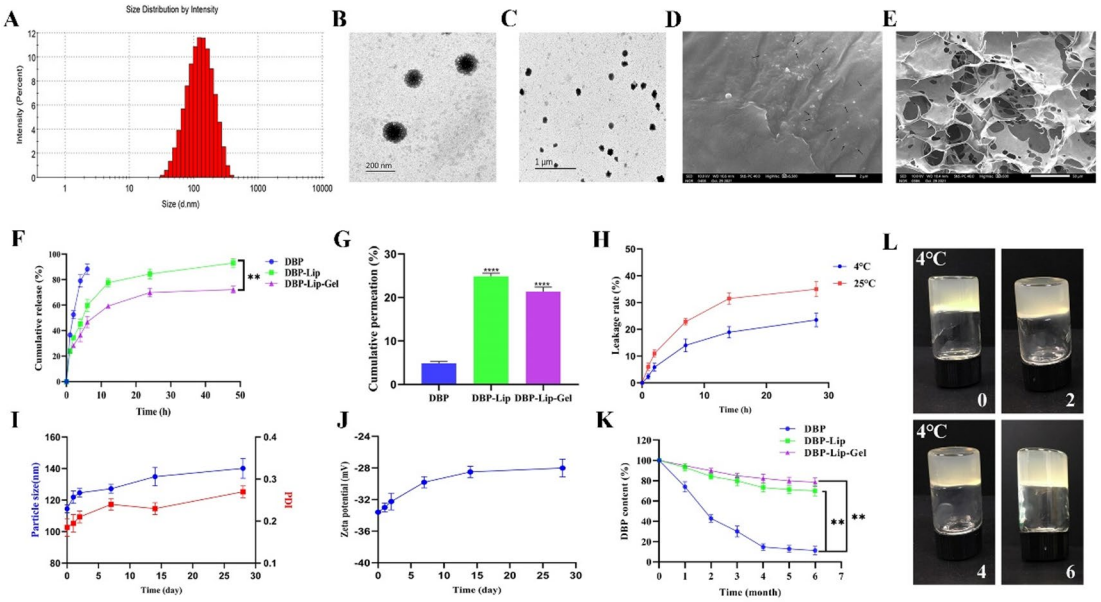

Fig. 2. Characterization of the DBP-Lip and DBP-Lip-Gel. (**A**) The particle size distribution of DBP-Lip measured using dynamic light scattering analysis. Transmission electron microscope images of DBP-Lip with the scale bar representing (**B**) 200 nm and (**C**) 1 μm. Scanning electron microscope images of the DBP-Lip-Gel with (**D**) 2 μm and (**E**) 50 μm. The arrows mark DBP-Lip uniformly distributed in the hydrogel. (**F**) The release profiles of different DBP formulations at 37 ℃ for 48 h. (**G**) The cumulative skin permeation of different DBP formulations. (**H**) Changes in leakage rate of DBP-Lip stored at 4 ℃ and 25 ℃ for 28 h. (**I**, **J**) Changes in particle size, PDI, and zeta potential of DBP-Lip for 28 days. (**K**) The DBP content of different DBP formulations stored for 6 months. (**L**) Visual appearance of DBP-Lip-Gel at predetermined time points of 0, 2, 4, and 6 months at 4 ℃. Data are expressed as the mean ± standard deviation; $^{**}p < 0.01$ DBP-Lip-Gel compared to the DBP-Lip group, $^{**}p < 0.01$ and $^{****}p < 0.0001$ compared to the DBP group, $n = 3$.

Group	Particle size	PDI	Zeta potential	EE (%)	DL (%)
Blank-Lip	98.7 ± 4.2	0.16 ± 0.03	− 28.43 ± 4.24	–	–
DBP-Lip	111.4 ± 2.8	0.18 ± 0.02	− 30.03 ± 3.16	84.6 ± 2.0	4.6 ± 0.2

Table 1. Characterization of DBP-Lip.

Skin permeation was evaluated using the Franz diffusion cells method. As shown in Fig. 2G, the cumulative skin permeation of free DBP solution was 4.87%, followed by that of DBP-Lip at 24.87% and that of DBP-Lip-Gel at 21.33%. The cumulative skin permeation of DBP-Lip was greater than that of free DBP solution ($p < 0.05$). Therefore, due to the convenience of simultaneous use, the DBP-Lip-Gel was deemed superior to the DBP-Lip. Results from the percutaneous penetration study demonstrated that the liposomal hydrogel delivery system was more effective for the topical application of DBP compared to using no delivery system.

Storage stability of DBP formulations

Changes in leakage rate, particle size, PDI, and zeta potential were used to evaluate the stability of DBP formulations. As shown in Fig. 2H, the leakage rate of DBP-Lip increased with time, increasing from 23.50% at 4 ℃ to 35.15% at 25 ℃ over 28 h. Furthermore, particle size and PDI of DBP formulations stored at 4 ℃ were slightly increased on the 28th day. The particle size of DBP-Lip changed from 114.1 nm to 140.0 nm, while the PDI changed from 0.19 to 0.27 (Fig. 2I). In addition, the zeta potential increased from − 33.6 mV to − 28.0 mV (Fig. 2J). These results indicated that liposomes deteriorate over time; however, lower temperatures can slow down the rate of deterioration.

The DBP content in different formulations stored at 4 ℃ for 6 months was also measured. As shown in Fig. 2K, the content in different formulations gradually decreased over time. At the end of the 6th month, the DBP content in free DBP, DBP-Lip, and DBP-Lip-Gel was 11.28%, 70.04% and 78.56%, respectively. The appearance of DBP-Lip-Gel stored at 4 ℃ for 6 months was captured. As shown in Fig. 2L, the colour, homogeneity, and fluidity of DBP-Lip-Gel had barely changed, indicating that the liposomal hydrogel maintained its physical character. These results indicated that the liposomal structure decreased the rate of DBP degradation. Moreover, the hydrogel provided anchoring sites for liposomes that further reduced the degradation rate.

In vitro cytotoxicity and cellular internalization

To verify the cell cytotoxicity with different DBP formulations, L929 cells were administered free DBP, DBP-Lip, and DBP-Lip-Gel and incubated for 24 h. Cell cytotoxicity was measured using CCK8 kits, and the results are shown in Fig. 3A. The cell viability with DBP-Lip was slightly higher than that with free DBP and DBP-Lip-Gel, and there was no significant difference in cell viability between free DBP and DBP-Lip-Gel. This indicated that liposomal formulation could promote the effects of DBP.

The cellular uptake efficiency with different formulations was determined by detecting the fluorescence of internalized RhB in L929 cells. The fluorescence intensity with each treatment is shown in Fig. 3B–C. The intracellular fluorescence of RhB-Lip and RhB-Lip-Gel was significantly higher than that in the free RhB group, which is attributable to the phospholipid bilayer structure. Nevertheless, the highest fluorescence was observed in the RhB-Lip group rather than in the RhB-Lip-Gel group, which suggested that the hydrogel delayed the release of its content under the same conditions. Therefore, the results indicated that the introduction of a liposome structure increased biocompatibility, resulting in increased cellular uptake compared to that in the non-liposome group.

Effects of DBP formulations on UVB-induced oxidative stress and cell damage

To examine the protective effect of DBPs and DBP formulations against UVB irradiation, L929 cells were pre-treated with different concentration of DBPs or DBP formulations before exposure to UVB irradiation. Cell viability and intracellular ROS were assessed using CCK8 kits and an ROS probe, respectively. As shown in Fig. 4A, UVB exposure significantly decreased the viability of L929 cells to 24.5%, whereas pre-treatment with different concentrations of DBPs increased cell viability in a dose-dependent manner. Furthermore, the free DBP, DBP-Lip and DBP-Lip-Gel rescued the cells from UVB-induced death, showing cell viabilities 6.2 times, 7.1 times and 6.5 times, respectively, that of UVB-induced cells (Fig. 4B).

UVB irradiation not only inhibits the viability of cells but also increases intracellular ROS. The ROS analysis was conducted under the same conditions as above using DCFH-DA, which resulted in green fluorescence in cells. As shown in Fig. 4C–D, green fluorescence in the UVB-induced group was much brighter, showing that intracellular ROS levels were 4.0 times higher than those of the control group. However, the intracellular ROS levels in the pre-treatment DBP group decreased relative to those in the UVB-induced group in a dose-dependent manner. In addition, DBP loaded into delivery systems (DBP-Lip and DBP-Lip-Gel) decreased intracellular ROS levels (Fig. 4E–F). Collectively, these data showed not only that DBP exhibited a protective effect against UVB-induced cell damage and intracellular ROS but also that use of a delivery system increase this protective effect.

Effects of DBP formulations on UVB-induced cell apoptosis

We investigated whether DBP, DBP-Lip, and DBP-Lip-Gel protected L929 cells from UVB-induced apoptosis. L929 cells were pre-treated with different concentrations of DBP or DBP-Lip, and DBP-Lip-Gel before exposure to UVB irradiation. Apoptosis was then analysis by annexin V and 7-AAD staining. As shown in Fig. 4G-H and

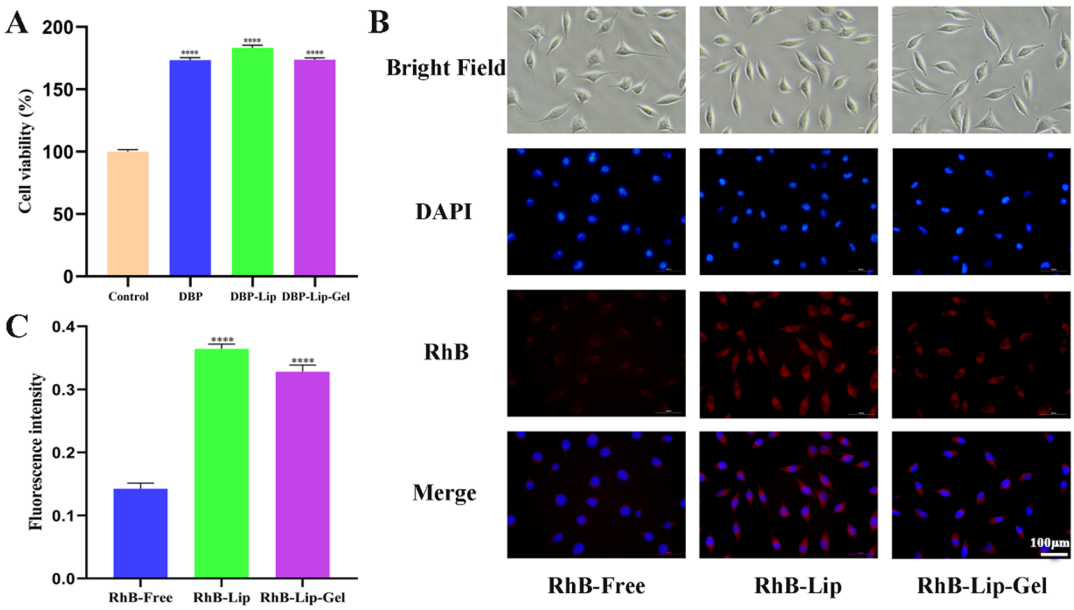

Fig. 3. In vitro cytotoxicity of different DBP formulation and intracellular uptake behaviours of free RhB, RhB-Lip, and RhB-Lip-Gel. (**A**) In vitro cytotoxicity in free DBP, DBP-Lip, and DBP-Lip-Gel groups at a DBP concentration of 4 mg/mL in L929 cells for 24 h. (**B**) Intracellular uptake behaviours of free RhB, RhB-Lip, and RhB-Lip-Gel in L929 cells at 6 h observed under a Nikon Ts2-FL fluorescence microscope. Scale bar, 100 μm. (**C**) Semi-quantitative fluorescence intensities with different RhB formulations in L929 cells. Data are presented as the mean ± standard deviation; $^{****}p < 0.0001$ compared to the control group or free RhB group, $n = 3$.

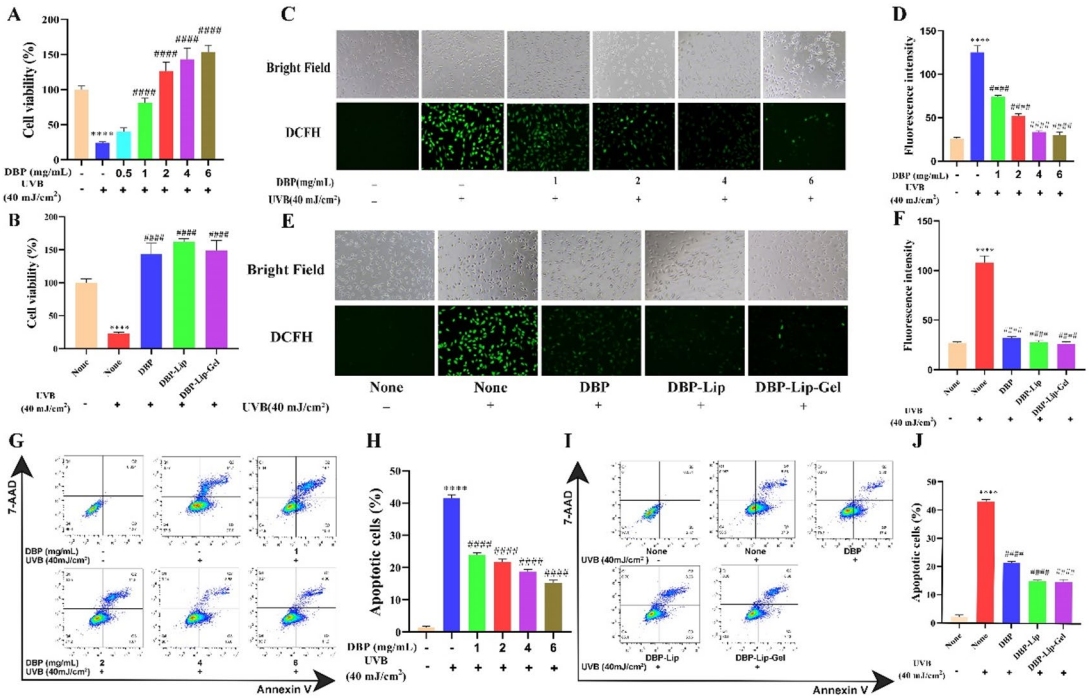

Fig. 4. The effects of DBPs at various doses and in various formulations on UVB-induced cytotoxicity, intracellular ROS production and anti-apoptotic effects. (**A**) Cytoprotective effect of DBP treatment on UVB-induced cytotoxicity in L929 cells. (**B**) Cytoprotective effect of DBP formulations on UVB-induced cytotoxicity in L929 cells. (**C**) Effects of DBPs at different doses on UVB-induced intracellular ROS production in L929 cells, with 40× magnification. (**D**) Quantification of fluorescence intensity of (**C**). (**E**) Effects of DBP formulations on UVB-induced intracellular ROS production in L929 cells, with 40× magnification. (**F**) Quantification of fluorescence intensity of (**E**). (**G**) Flow cytometric analysis of DBP on anti-apoptosis effects in UVB-irradiated L929 cells. (**H**) Quantification of (**G**). (**I**) Flow cytometric analysis of DBP formulations on anti-apoptosis effects in UVB-irradiated L929 cells. (**J**) Quantification of (**I**). Data are presented as the mean ± standard deviation; $^{****}p < 0.0001$ compared to non-UVB irradiation group, $^{\#\#\#\#}p < 0.0001$ compared to the UVB irradiation and non-DBP treatment group, $n = 3$.

Fig. S1, UVB irradiation induced 41.5% cell apoptosis, whereas pre-treatment with DBP significantly decreased UVB-induced cell apoptosis in a dose-dependent manner. In addition, DBP-Lip and DBP-Lip-Gel rescued UVB-induced cell apoptosis, decreasing cell apoptosis to 15.0% and 14.8%, respectively (Fig. 4I-J). Collectively, these results indicated that DBP exhibited a protective effect against UVB-induced apoptosis. Furthermore, the designed delivery systems of DBP-Lip, and DBP-Lip-Gel for DBP showed a better protective effect than free DBP.

DBP suppression of UVB-induced photoaging of skin

Images were captured to document the pathological changes in the skin before the mice were sacrificed. As shown in Fig. 5A, after three weeks of UVB irradiation, the mice in the UVB irradiation group exhibited severe erythema on their dorsal skin. In contrast, the dorsal skin of the Vc group and the DBP administration groups remained smooth, indicating that DBP had a protective effect against UVB irradiation. By the 6th week, all groups showed more pronounced erythema than at the 3rd week. However, the skin changes in the DBP-Lip-Gel-High group were minimal and comparable to those in the Vc group. By the 9th week, the skin of the UVB-irradiated mice displayed more severe erythema and wrinkles compared to the non-irradiated mice. According to relevant literature[45,46], the skin wrinkles was scored (Table S2). As shown in Fig. S2, the UVB irradiation resulted in the deterioration of wrinkle formation. However, the wrinkles score of the DBP administration and Vc group was reduced. Among these, the DBP-Lip-H group demonstrated a stronger protective effect than the free DBP group. Notably, the DBP-Lip-Gel group exhibited the best protection against photoaging of all the DBP administration groups. Both the high and low dose DBP-Lip-Gel groups showed no erythema or wrinkles, similar to the Vc and normal group. These results indicated that DBP effectively protects the skin from UVB irradiation, especially when delivered in the DBP-Lip-Gel formulation. Additionally, as shown in Fig. 5B-C, none of the administration groups had an adverse effect on body weight or organ coefficients in mice.

Histopathology analysis of skin characteristics

After the mice were euthanized, dorsal skin tissues were harvested and analyzed using HE, Masson's, and EVG stains. As shown in Fig. 5D-E, the epidermal thickness in the UVB irradiation group was significantly greater than that in the non-irradiated group. Conversely, the epidermal thickness was reduced to varying degrees in all DBP treatment groups compared to the UVB irradiation group. Specifically, the epidermal thickness in the

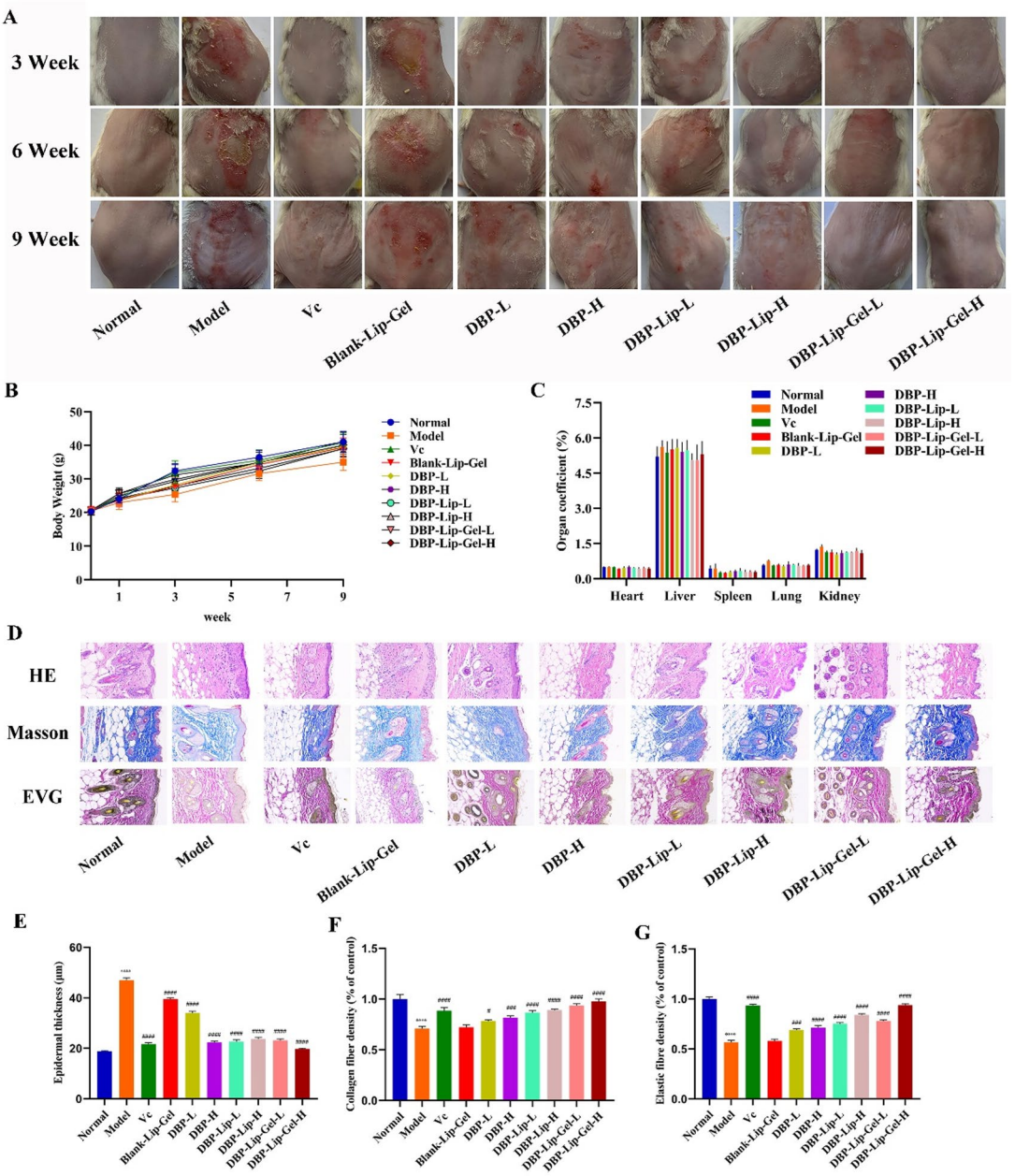

Fig. 5. Effects of different DBP formulations on UVB-induced skin photoaging in ICR mice. (**A**) Morphological changes in ICR mice following UVB irradiation with various DBP formulations, $n = 6$. (**B**) Body weight changes under UVB irradiation over 9 weeks with different DBP formulations, $n = 6$. (**C**) Organ coefficients of ICR mice exposed to UVB irradiation with various DBP formulations, $n = 6$. (**D**) HE, Masson's trichrome, and EVG staining to examine epidermal thickness (**E**), collagen distribution (**F**), and elastic fibre distribution (**G**), with 100× magnification. Data are presented as the mean ± standard deviation; $^{****}p < 0.0001$ compared to the normal group; $^{\#}p < 0.05$, $^{\#\#\#}p < 0.001$, and $^{\#\#\#\#}p < 0.0001$ compared to the Model group, $n = 3$.

DBP-H group was similar to that in the DBP-Lip groups and the DBP-Lip-Gel-L group, and it was significantly thinner than that in the Model group. Furthermore, the epidermal thickness in the DBP-Lip-Gel-H group was the thinnest, even thinner than that of the Vc group. These results indicate that DBP effectively inhibits UVB-induced epidermal thickening, with the DBP-Lip-Gel formulation showing the most pronounced effect.

Collagen expression levels were assessed via Masson's staining. The average collagen content was notably diminished in the UVB irradiation group relative to the non-irradiated group. However, administration of DBP effectively restored collagen expression in the mouse dermis, which had been reduced by UVB irradiation (Fig. 5F). Within the same DBP formulation, the collagen content in the high-dose group was superior to that in the low-dose group. Additionally, at equivalent doses of DBP, the collagen content in the DBP-Lip-Gel group surpassed that in the DBP-Lip group, which in turn exceeded that in the free DBP group. Notably, the DBP-Lip-Gel-H group demonstrated the most robust protective ability for collagen.

EVG staining revealed a trend similar to that observed with Masson's staining. The expression levels of elastic fibers were reduced in the UVB irradiation group (Fig. 5G); however, these detrimental effects were reversed in the DBP administration group. In the DBP, DBP-Lip, and DBP-Lip-Gel groups, the content of elastic fibers increased proportionally with the dose of DBP. Furthermore, at the same DBP dose, the elastic fiber content in the DBP-Lip-Gel group was higher than that in the DBP-Lip group, which was in turn higher than that in the free DBP group. These results indicate that DBP regulates elastic fiber content in a dose-dependent manner, with the high dose of DBP-Lip-Gel significantly enhancing elastic fiber content.

In summary, DBP mitigated UVB-induced skin damage by regulating the expression of collagen and elastic fibers, as well as modulating epidermal thickness.

Production of pro-inflammatory cytokines in a UVB-irradiated mouse model

UVB irradiation was accompanied by inflammatory cell infiltration and proinflammatory factor secretion[47]. Therefore, we examined the expression of pro-inflammatory factors and found that, compared with the non-irradiated group, UVB irradiation significantly increased the expression of pro-inflammatory cytokines in serum containing IL-1, IL-6, and TNF-α (Fig. 6A–C), consistent with the results of previous studies[48]. Moreover, the increased levels of IL-1, IL-6, and TNF-α induced by UVB irradiation were reversed by DBP treatment. This effect was most pronounced in the DBP-Lip-Gel group, with DBP treatment at either a low or high dose significantly decreasing the expression levels of these pro-inflammatory cytokines compared with the UVB irradiation alone.

A similar protective effect was observed in mouse dorsal skin, as shown in Fig. 6D–F. Various pro-inflammatory cytokines were significantly increased in the UVB irradiation group compared with those in

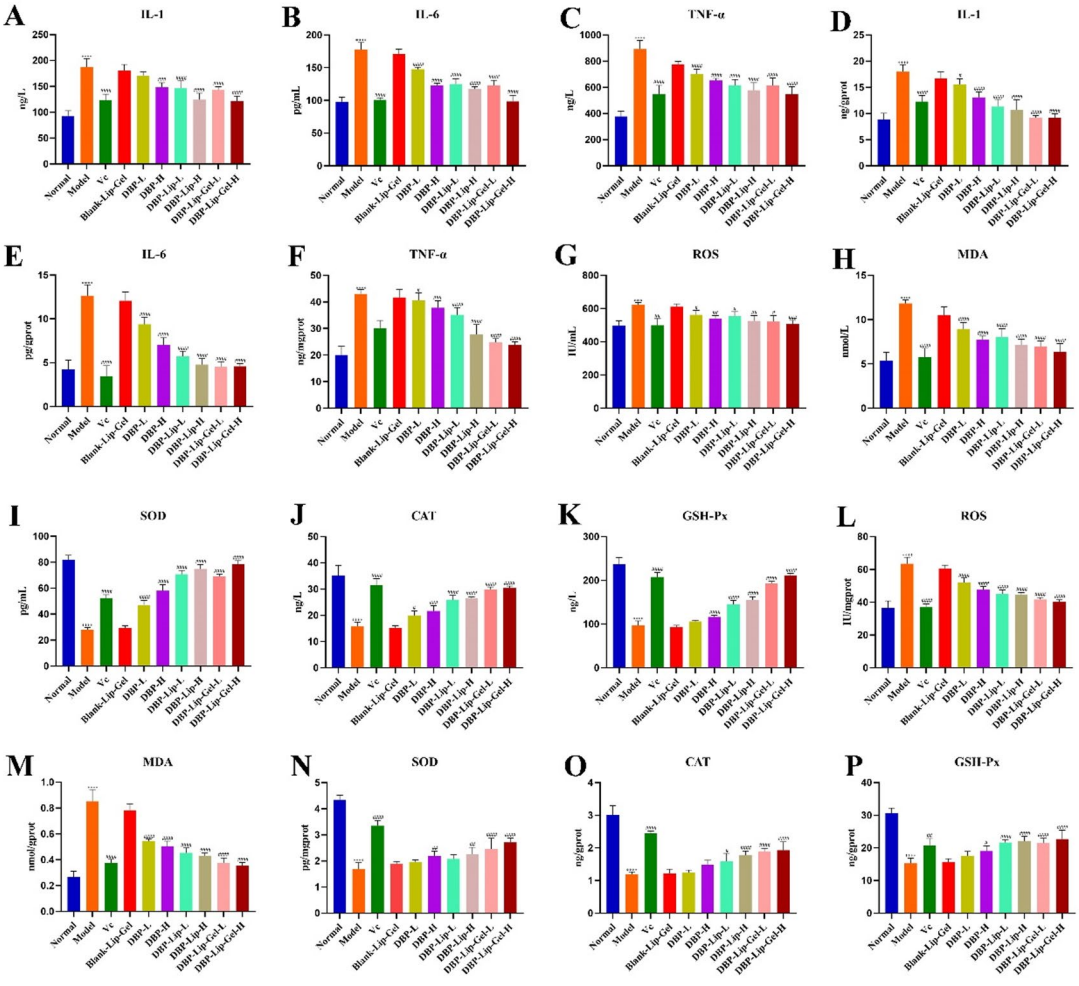

Fig. 6. Effects of DBP formulations on inflammatory cytokines and oxidative stress response in mouse serum and skin tissue. IL-1 (**A**), IL-6 (**B**), and TNF-α (**C**) in mouse serum were measured using ELISA kits. IL-1 (**D**), IL-6 (**E**), and TNF-α (**F**) in mouse dorsal skin tissue were measured using ELISA kits. ROS (**G**), MDA (**H**), SOD (**I**), CAT (**J**), and GSH-Px (**K**) in mouse serum were measured using ELISA kits. ROS (**L**), MDA (**M**), SOD (**N**), CAT (**O**), and GSH-Px (**P**) in mouse dorsal skin tissue were measured using ELISA kits. Data are presented as the mean ± standard deviation; $^{***}p < 0.001$ and $^{****}p < 0.0001$ compared to the normal group; $^{\#}p < 0.05$, $^{\#\#}p < 0.01$, $^{\#\#\#}p < 0.001$, and $^{\#\#\#\#}p < 0.0001$ compared to the Model group, $n = 3$.

the non-irradiated group. Furthermore, DBP administration significantly reduced the expression of these pro-inflammatory cytokines. However, the different formulations showed the same result: high-dose administration had a greater protective effect than low-dose administration. Among all groups, the high dose of DBP-Lip-Gel showed the strongest protective effect against inflammatory reactions.

Oxidative stress production and antioxidant enzyme activity in a UVB-irradiated mouse model

Oxidative stress is recognized as the primary response to UVB irradiation. Therefore, we examined the level of ROS, MDA, and relative antioxidative enzyme activity in serum and skin tissue. UVB irradiation significantly increased the expression level of ROS in both serum and skin tissue (Fig. 6G, L). MDA, acting as an indicator of lipid peroxidation, was significantly increased in the UVB irradiation group compared with the non-irradiated group (Fig. 6H, M). However, in the DBP, DBP-Lip and DBP-Lip-Gel groups, the ROS level and MDA decreased with the increase of DBP dose, and were lower than that in the Model group. Furthermore, the ROS level and MDA of DBP-Lip-Gel group were lower than those in DBP-Lip group, while the ROS level and MDA of DBP-Lip group were lower than those of free DBP group. The high dose of DBP-Lip-Gel significantly reversed the increase in ROS and MDA induced by UVB irradiation.

We also examined the antioxidant enzyme activities of SOD, CAT, and GSH-Px in both serum and skin tissue. Contrary to the results of ROS and MDA, the activities of the three antioxidant enzymes were decreased by following UVB irradiation (Fig. 6I-K, N-P). However, DBP administrations reversed the decrease of antioxidant enzymes induced by UVB irradiation in all DBP treatment groups in a dose-dependent manner. The DBP-Lip-Gel group showed the strongest protective effect and statistically significant differences in enzyme activities compared with those in the Model group.

UVB-induced cell apoptosis in a UVB-irradiated mouse model

To further examine the potential mechanism of protection by DBP against UVB irradiation, we determined the expression levels of apoptosis- or cell growth-related proteins by western blot. We found that DBP inhibited the expression level of pro-apoptotic proteins of Bax and caspase-3 induced by UVB irradiation and reversed the expression of antiapoptotic protein Bcl-2, which was inhibited by UVB irradiation (Fig. 7A–D and Fig. S3). Moreover, consistent with the HE staining data, the expression level of I type collagen (COL1A1) was

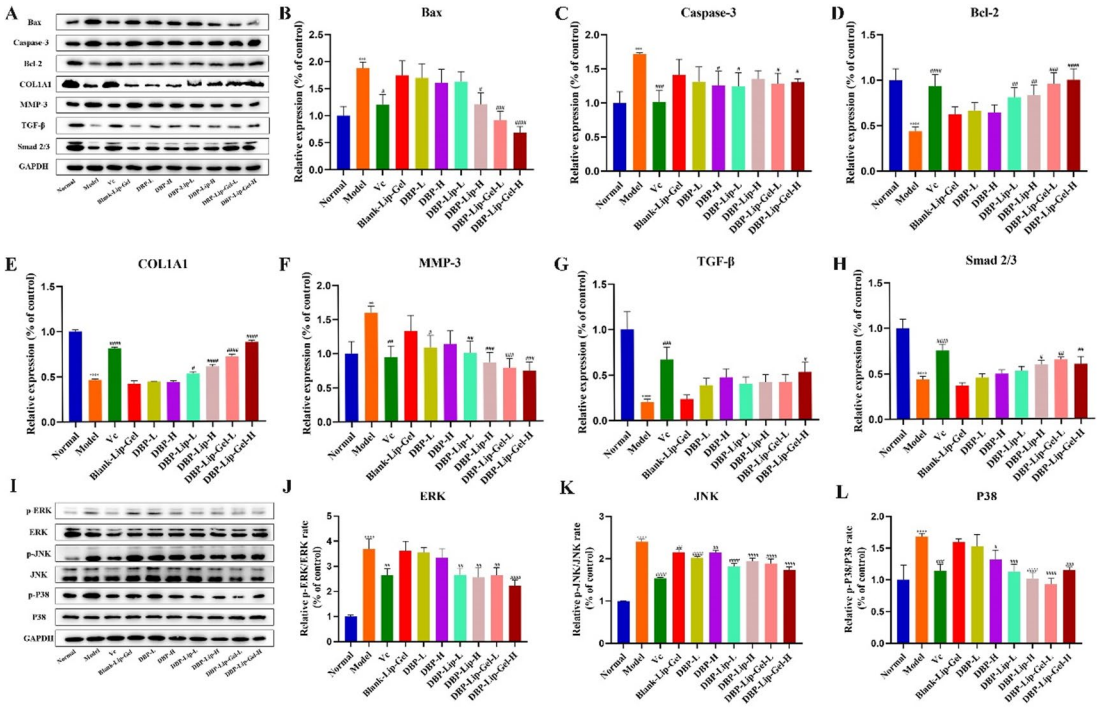

Fig. 7. Effects of different DBP formulations on the protein expression and phosphorylation of MAPKs in mouse dorsal skin tissues. (**A**) Representative immunoblots of Bax, Bcl-2, Caspase-3, COL1A1, MMP-3, TGF-β, Smad2/3, and GAPDH proteins. (**B**) The relative expression of Bax quantities. (**C**) The relative expression of Caspase-3 quantities. (**D**) The relative expression of Bcl-2 quantities. (**E**) The relative expression of COL1A1 quantities. (**F**) The relative expression of MMP-3 quantities. (**G**) The relative expression of TGF-β quantities. (**H**) The relative expression of Smad2/3 quantities. (**I**) Representative immunoblots and phosphorylation levels of ERK, JNK, P38, and GAPDH proteins. (**J**) The relative ratio of p-ERK/ERK quantities. (**K**) The relative ratio of p-JNK/JNK quantities. (**L**) The relative ratio of p-P38/P38 quantities. Data are presented as the mean ± standard deviation; $^{**}p < 0.01$, $^{***}p < 0.001$, and $^{****}p < 0.0001$ compared to the normal group; $^{\#}p < 0.05$, $^{\#\#}p < 0.01$, $^{\#\#\#}p < 0.001$, and $^{\#\#\#\#}p < 0.0001$ compared to the Model group, $n = 3$.

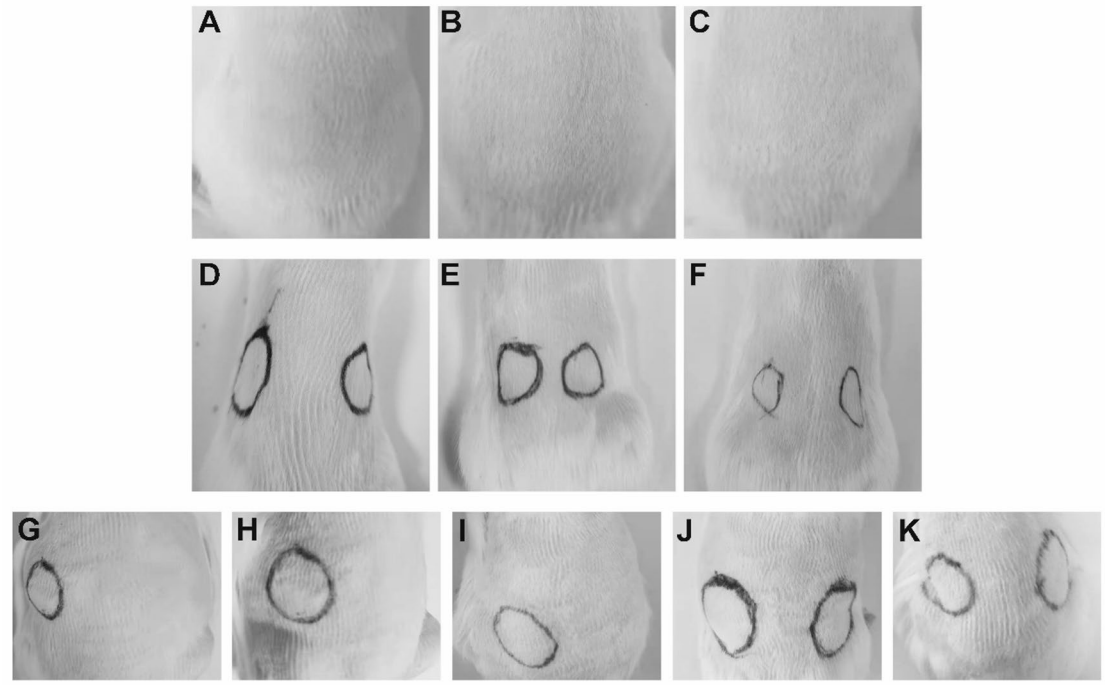

Fig. 8. Skin safety studies of the DBP-Lip-Gel formulation. Representative photographs of the dorsal skin of healthy SD rats on day 0 (**A**), day 7 (**B**), and day 14 (**C**) of an acute dermal toxicity test, $n = 6$. Representative photographs of the dorsal skin of healthy SD rats on day 0 (**D**), day 7 (**E**), and day 14 (**F**) of a multiple skin irritation test, $n = 6$. Representative photographs of the dorsal skin of healthy adult guinea pigs following induced contact on day 0 (**G**), day 7 (**H**), and day 14 (**I**) and stimulated contact on days 29 (**J**) and 30 (**K**) of skin sensitization test, $n = 10$.

significantly downregulated in response to UVB irradiation; however, DBP reversed this phenomenon (Fig. 7E), especially in the high dose of DBP-Lip-Gel group, where the changes of UVB-induced protein expression were more strongly inhibited. In addition, the expression level of MMP-3 induced by UVB irradiation was reversed with DBP administration (Fig. 7F). Meanwhile, the expression levels of TGF-β and Smad 2/3 were significantly downregulated by UVB irradiation (Fig. 7G–H); DBP reversed these phenomena. These results are consistent with previous reports[49], UVB irradiation induced increased expression of pro-apoptotic proteins Bax and caspase-3 in concert with the repression of antiapoptotic proteins Bcl-2, while accompanied by collagen loss and an increase of MMPs. After various treatments, the changes in protein expression induced by UVB irradiation were improved. In our study, we revealed that treatment with DBP protected against UVB-induced apoptosis and collagen degradation by inhibiting the expression of MMP-3. In particular, the high dose of DBP-Lip-Gel significantly decreased expression of pro-apoptotic proteins Bax and caspase-3, while increasing the expression of antiapoptotic protein Bcl-2. At the same time, DBP-Lip-Gel down-regulated MMP-3 and increased the expression of COL1A1 by activating TGF/Smad signaling pathway.

UVB irradiation protection through MAPK signaling in a UVB-irradiated mouse model

We sought to investigate whether the MAPK signalling pathway was involved in UVB-induced cell apoptosis by measuring the activity of transduction signalling MAPK-related proteins, which are downstream of intracellular ROS and cytokines (Fig. 7I and Fig. S4). Compared to the normal group, UVB irradiation resulted in increased phosphorylation of ERK, JNK, and P38 in the UVB irradiation group (Fig. 7J-L). However, compared to the UVB-irradiated group, treatment with DBP, DBP-Lip and DBP-Lip-Gel inhibited phosphorylation of MAPK pathway members ERK, JNK, and P38, especially the DBP-Lip-Gel groups exhibited the strongest inhibition effect. Similarly to the studies which have shown that low-molecular-weight peptides can protect skin aging by acting through the MAPK and TGF signaling pathways[17].

Accordingly, these data suggested that DBP treatment protected skin against UVB irradiation by suppressing MAPK pathway members ERK, JNK, and P38 activation. Furthermore, DBP-Lip-Gel exhibited the best protection effect.

Skin safety of DBP formulations

For acute dermal toxicity testing, DBP-Lip-Gel was smeared on the dorsal skin of healthy SD rats for 14 days. The dorsal skin, hair, and behavioural activity of rats were monitored and photographed. As shown in Fig. 8A–C, all rats exhibited normal health without any skin pathological changes, indicating that DBP-Lip-Gel had no acute dermal toxicity.

For multiple skin irritation testing, DBP-Lip-Gel was smeared on the left side and Blank-Lip-Gel on the right side of the dorsal skin of SD rats. As shown in Fig. 8D–F, the left side dorsal skin did not exhibit erythema or oedema after topical administration of DBP-Lip-Gel for 14 days, indicating that the DBP-Lip-Gel was safe for topical utilization.

For skin sensitization testing, DBP-Lip-Gel was smeared on the back dorsal skin of guinea pigs, and the skin was photographed after 6 h of administration at predetermined time points on days 0, 7, 14, 28, and 30. As shown in Fig. 8G–K, there was no erythema or oedema in the test area after DBP-Lip-Gel treatment, indicating that DBP-Lip-Gel did not cause a sensitization reaction and was safe for topical administration.

Discussion

Maintaining skin health is gaining increasing attention. When the skin is exposed to UV irradiation, it suffers various physiological lesions, and the body initiates diverse defense mechanisms to prevent damage. ROS production is considered the primary response to UV irradiation. An increase in intracellular ROS levels induces an increase in MDA, leading to subsequent oxidative stress and damage to cells and tissues[50]. Antioxidant substances have been effectively used to control oxidative stress and validate responses[51].

We investigated whether peptides from deer blood have an antioxidative effect in cells and a mouse model following UVB irradiation. First, we characterized the peptides extracted from deer blood. The molecular weight distribution of DBPs was below 7.8 KDa, indicating that the peptides we harvested were of low molecular weight. We also examined the amino acid content as a nutritional parameter of DBPs. Results showed that essential amino acids and hydrophobic amino acids accounted for 40.44% and 49.60% of total amino acids, respectively. Combined with antioxidant activity analysis, these findings indicated that DBP was rich in nutrients and possessed high antioxidative activity, which can contribute to the maintenance of skin health.

Due to the instability of peptides in an aqueous solution, we designed a novel liposomal-hydrogel complex delivery system that combines the advantages of liposomes for biocompatibility and hydrogel for application. Characterization results showed that DBP-Lip had a uniform spherical structure, stable storage properties, and was uniformly distributed in the hydrogel, which had a loose porous network structure providing anchoring sites for the liposome.

To clarify the value of the delivery system, we first examined the cellular uptake of different formulations. Results showed that the strongest fluorescence signal was in the liposome group, and a stronger signal was detected in the hydrogel leaching solution group than in the water-soluble substance group, indicating that the lipid bilayer structure of liposomes promoted cell uptake. Furthermore, we examined skin permeation with different formulations. Data showed that cumulative permeation with the liposome group was the highest, followed by the liposomal-hydrogel group, indicating that the liposome component of the delivery system promotes absorption into skin cells.

To further evaluate formulation properties, we assessed in vitro release and storage stability with different DBP formulations. In vitro release of DBP-Lip was slow, exhibiting no burst release, suggesting that all ingredients were encapsulated within the liposome rather than displayed on the outer surface. Additionally, DBP-Lip-Gel was more suitable for preservation at 4 ℃, showing a slow decrease in DBP content.

In vitro cell cytotoxicity studies of different DBP formulations indicated that DBP promoted cell proliferation in a dose-dependent manner. At a dose of 6 mg/mL, the proliferation rate increased 2.0 times compared to the normal group, indicating that DBP not only showed no toxicity but also promoted proliferation. Moreover, we observed dose-dependent DBP reversal of cell cytotoxicity induced by UV irradiation, with DBP-Lip showing the best effect. UVB irradiation increased intracellular ROS[52], whereas DBP reversed the increase in ROS induced by UVB irradiation in a dose-dependent manner. The DBP formulations had a better effect than free DBP. Additionally, UVB irradiation induced cell apoptosis[53], and we found the UVB-induced apoptosis in cells up to 41.5%. Administration of DBP or DBP formulations rescued cells from apoptosis. These results indicated that DBP had protective effects against UVB-induced damage, with DBP-Lip-Gel showing the most pronounced protective effect.

For in vivo validation, we established a photoaging mouse model to investigate the protective effects of DBP and different DBP formulations. UVB irradiation induce wrinkles and erythema in mouse dorsal skin, whereas DBP in different formulations significantly rescued the skin from injury. UVB irradiation induced skin injury through several deleterious signaling pathways, including apoptosis, inflammation, ROS production, and collagen degradation. Analysis of pro-inflammatory factors indicated that impaired skin following UVB irradiation resulted in an inflammatory response, which DBP administration reversed. Analysis of oxidative stress factors such as ROS, antioxidant enzymes, and MDA by ELISA showed that UVB irradiation upregulated ROS and MDA and downregulated antioxidant enzyme expression. DBP reversed these changes, regulating the expression of ROS and cytokines. Among all treatment groups, DBP-Lip-Gel exhibited the best protective effect, significantly reducing the oxidative stress response and inflammatory response induced by UVB irradiation.

Based on our results, we investigated downstream signaling pathways related to oxidative stress, apoptosis, and wrinkle formation. DBPs inhibited the expression of pro-apoptotic proteins Bax and caspase-3, while reversing the UVB-induced decrease in the anti-apoptotic protein Bcl-2. Previous studies have reported that the MAPK and TGF-β pathways play key roles in signal transduction following UVB irradiation[54]. Our results showed that DBPs suppressed the phosphorylation of ERK, JNK, and P38 induced by UVB exposure. Additionally, DBPs reduced MMP-3 expression and attenuated collagen degradation. DBP treatment also restored TGF/Smad signaling by upregulating TGF-β and Smad2/3 expression[55]. These effects collectively led to increased type I collagen synthesis and decreased MMP expression.

Overall, DBPs mitigated wrinkle formation and skin damage associated with photoaging by restoring collagen content and improving extracellular matrix structure through modulation of these signaling pathways.

Although this study provides a comprehensive analysis of DBPs in photoaging treatment, certain limitations remain, including the lack of human data, potential variability in deer blood composition, and the absence of long-term safety evaluations. These aspects will be addressed in future research.

Conclusion

In this study, we demonstrated that deer blood peptides (DBPs) exhibit significant photoprotective effects and developed a liposomal-hydrogel DBP formulation for topical use to shield the skin from UV irradiation. DBPs are rich in antioxidants and enhance cell proliferation. The DBP-Lip formulation is stable, promotes skin penetration, and enhances cellular uptake. Topical application of DBP-Lip-Gel provided optimal skin protection by reducing inflammation, apoptosis, and boosting the expression of various antioxidant enzymes. Additionally, DBP's protective effects are mediated through the MAPK/TGF signaling pathway, decreasing MMP3 expression and collagen degradation. Overall, DBP-Lip-Gel shows promising potential for medical applications.

Data availability

The data used within the manuscript are available from the corresponding author (Jin Pei) on reasonable request.

Received: 5 June 2025; Accepted: 28 October 2025
Published online: 26 November 2025

References

1. Fernando, I. et al. Fucoidan fractionated from sargassum Coreanum via step-gradient ethanol precipitation indicate promising uvb-protective effects in human keratinocytes. *Antioxid. (Basel)*. **10**, 347 (2021).
2. Yang, Y., Wang, X. & Wang, P. Signaling mechanisms underlying lymphatic vessel dysfunction in skin aging and possible anti-aging strategies. *Biogerontology* **24**, 727–740 (2023).
3. Jo, K. et al. An anthocyanin-enriched extract from vaccinium uliginosum improves signs of skin aging in uvb-induced photodamage. *Antioxid. (Basel)*. **9**, 844 (2020).
4. Stiefel, C. & Schwack, W. Photoprotection in changing times - uv filter efficacy and safety, sensitization processes and regulatory aspects. *Int. J. Cosmet. Sci.* **37**, 2–30 (2015).
5. Calo, R., Visone, C. M. & Marabini, L. Thymol and thymus vulgaris l. Activity against uva- and uvb-induced damage in Nctc 2544 cell line. *Mutat. Res. Genet. Toxicol. Environ. Mutagen.* **791**, 30–37 (2015).
6. Lin, M. J., Lin, P., Wen, K. C., Chiang, H. M. & Lu, M. C. Jelly Fig (ficus Awkeotsang makino) exhibits antioxidative and anti-inflammatory activities by regulating reactive oxygen species production via Nfkappab signaling pathway. *Antioxid. (Basel)*. **11**, 981 (2022).
7. Okon, I. S. & Zou, M. H. Mitochondrial Ros and cancer drug resistance: implications for therapy. *Pharmacol. Res.* **100**, 170–174 (2015).
8. Xu, T. et al. Oxidative stress in cell death and cardiovascular diseases. *Oxid Med Cell Longev.* 9030563 (2019). (2019).
9. Aldosari, S., Awad, M., Harrington, E. O., Sellke, F. W. & Abid, M. R. Subcellular reactive oxygen species (ros) in cardiovascular pathophysiology. *Antioxid. (Basel)*. **7**, 14 (2018).
10. Venza, I. et al. Ros as regulators of cellular processes in melanoma. *Oxidative Medicine and Cellular Longevity.* 1208690 (2021). (2021).
11. Park, C. P., Kim, J., Kim, W. J., Cheong, W. & Kim, H. Malonic acid isolated from Pinus densiflora inhibits uvb-induced oxidative stress and inflammation in Hacat keratinocytes. *Genes (Basel)*. **13**, 816 (2021).
12. Yang, L., An, L., Wang, Y. & Li, J. Protective effect of isopsoralen on uvb-induced injury in Hacat cells via the Er and p38 Mapk signaling pathways. *J. Food Biochem.* **46**, e14163 (2022).
13. Zhi, Q. et al. The anthocyanin extracts from purple-fleshed sweet potato exhibited anti-photoaging effects on ultraviolent b-irradiated balb/c-nu mouse skin. *J. Funct. Foods.* **64**, 103640 (2020).
14. Wang, L., Je, J. G., Yang, H. W., Jeon, Y. J. & Lee, S. Dieckol, an algae-derived phenolic compound, suppresses uvb-induced skin damage in human dermal fibroblasts and its underlying mechanisms. *Antioxid. (Basel)*. **10**, 352 (2021).
15. Kunchana, K., Jarisarapurin, W., Chularojmontri, L. & Wattanapitayakul, S. K. Potential use of Amla (phyllanthus emblica l.) fruit extract to protect skin keratinocytes from inflammation and apoptosis after Uvb irradiation. *Antioxid. (Basel)*. **10**, 703 (2021).
16. Peng, Z. et al. Ameliorative effects of peptides from the oyster (crassostrea hongkongensis) protein hydrolysates against uvb-induced skin photodamage in mice. *Mar. Drugs.* **18**, 288 (2020).
17. Bang, J., Jin, Y. & Choung, S. Low molecular polypeptide from oyster hydrolysate recovers Photoaging in skh-1 hairless mice. *Toxicol. Appl. Pharmacol.* **386**, 114844 (2020).
18. Toldra, F., Mora, L. & Reig, M. New insights into meat by-product utilization. *Meat Sci.* **120**, 54–59 (2016).
19. Chang, C., Wu, K. & Chiang, S. Antioxidant properties and protein compositions of Porcine haemoglobin hydrolysates. *Food Chem.* **100**, 1537–1543 (2007).
20. Bah, C., Carne, A. B., McConnell, M. & A. & Composition and biological activities of slaughterhouse blood from red deer, sheep, pig and cattle. *J. Sci. Food Agric.* **96**, 79–89 (2016).
21. Liu, D. et al. Inhibition of growth and metastasis of breast cancer by targeted delivery of 17-hydroxy-jolkinolide b via hyaluronic acid-coated liposomes. *Carbohydr. Polym.* **257**, 117572 (2021).
22. Si, Y. et al. Targeted liposomal chemotherapies to treat triple-negative breast cancer. *Cancers (Basel)*. **13**, 3749 (2021).
23. Verma, D., Verma, S., Blume, G. & Fahr, A. Liposomes increase skin penetration of entrapped and non-entrapped hydrophilic substances into human skin: A skin penetration and confocal laser scanning microscopy study. *Eur. J. Pharm. Biopharm.* **55**, 271–277 (2003).
24. Sakdiset, P., Okada, A., Todo, H. & Sugibayashi, K. Selection of phospholipids to design liposome preparations with high skin penetration-enhancing effects. *J. Drug Deliv. Sci. Technol.* **44**, 58–64 (2018).
25. Elnaggar, Y., El-Refaie, W., El-Massik, M. & Abdallah, O. Lecithin-based nanostructured gels for skin delivery: an update on state of Art and recent applications. *J. Control Release.* **180**, 10–24 (2014).
26. Guan, Y. et al. Propranolol hydrochloride-loaded liposomal gel for transdermal delivery: characterization and in vivo evaluation. *Int. J. Pharm.* **487**, 135–141 (2015).
27. Song, H., Meng, M., Cheng, X., Li, B. & Wang, C. The effect of collagen hydrolysates from silver carp (hypophthalmichthys molitrix) skin on uv-induced Photoaging in mice: molecular weight affects skin repair. *Food Funct.* **8**, 1538–1546 (2017).
28. Fu, Y. et al. The protective effect of collagen peptides from Bigeye tuna (thunnus obesus) skin and bone to attenuate uvb-induced Photoaging via Mapk and tgf-β signaling pathways. *J. Funct. Foods.* **93**, 105101 (2022).
29. Abeyrathne, E. D., Lee, H. Y., Jo, C., Suh, J. W. & Ahn, D. U. Enzymatic hydrolysis of ovomucin and the functional and structural characteristics of peptides in the hydrolysates. *Food Chem.* **192**, 107–113 (2016).

30. Nurilmala, M., Hizbullah, H. H., Karnia, E., Kusumaningtyas, E. & Ochiai, Y. Characterization and antioxidant activity of collagen, gelatin, and the derived peptides from Yellowfin tuna (thunnus albacares) skin. *Mar. Drugs*. **18**, 98 (2020).
31. Zhang, C., Song, X., Cui, W. & Yang, Q. Antioxidant and anti-ageing effects of enzymatic polysaccharide from pleurotus eryngii residue. *Int. J. Biol. Macromol.* **173**, 341–350 (2021).
32. Chen, X. et al. Fullerenol protects cornea from ultraviolet b exposure. *Redox Biol.* **54**, 102360 (2022).
33. Xie, Y. et al. A novel estrogen-targeted pegylated liposome co-delivery oxaliplatin and Paclitaxel for the treatment of ovarian cancer. *Biomed. Pharmacother.* **160**, 114304 (2023).
34. Houlleberghs, M. et al. Magneto-hydrodynamic mixing: A new technique for Preparing carbomer hydrogels. *AIChE J.* **69**, e17911 (2022).
35. Luo, M. et al. Preparation, stability and antioxidant capacity of nano liposomes loaded with procyandins from lychee pericarp. *J. Food Eng.* **284**, 110065 (2020).
36. Zhou, T. et al. Preparation, characterization, and in vivo evaluation of nk4-conjugated hydroxycamptothecin-loaded liposomes. *Int. J. Nanomed.* **15**, 2277–2286 (2020).
37. Caddeo, C. et al. Tocopherol-loaded transfersomes: in vitro antioxidant activity and efficacy in skin regeneration. *Int. J. Pharm.* **551**, 34–41 (2018).
38. Liu, Y., Liu, D., Zhu, L., Gan, Q. & Le, X. Temperature-dependent structure stability and in vitro release of chitosan-coated Curcumin liposome. *Food Res. Int.* **74**, 97–105 (2015).
39. Dragicevic, N., Krajisnik, D., Milic, J., Fahr, A. & Maibach, H. Development of hydrophilic gels containing coenzyme q_{10}-loaded liposomes: Characterization, stability and rheology measurements. *Drug Dev. Ind. Pharm.* **45**, 43–54 (2019).
40. Silva, B., Peloi, K., Ximenes, V., Nakamura, C. & Lautenschlager, S. 2-acetylphenothiazine protects l929 fibroblasts against uvb-induced oxidative damage. *J. Photochem. Photobiol., B.* **216**, 112130 (2021).
41. Daliri, E. B., Oh, D. H. & Lee, B. H. Bioactive peptides. *Foods* **6**, 32 (2017).
42. Christodouleas, D., Fotakis, C., Nikokavoura, A., Papadopoulos, K. & Calokerinos, A. Modified Dpph and Abts assays to assess the antioxidant profile of untreated oils. *Food. Anal. Methods*. **8**, 1294–1302 (2014).
43. Lian, B. et al. Galactose modified liposomes for effective co-delivery of doxorubicin and combretastatin a4. *Int. J. Nanomed.* **16**, 457–467 (2021).
44. Li, Y. et al. Long-circulating thermosensitive liposomes for the targeted drug delivery of oxaliplatin. *Int. J. Nanomed.* **15**, 6721–6734 (2020).
45. Budluang, P. et al. N-benzyl-n-methyldecane-1-amine derived from Garlic ameliorates uvb-induced Photoaging in Hacat cells and skh-1 hairless mice. *Sci. Rep.* **15**, 6979 (2025).
46. Bissett, D. L., Hannon, D. P. & Orr, T. V. An animal model of solar-aged skin: Histological, physical, and visible changes in uv-irradiated hairless mouse skin. *Photochem. Photobiol.* **46**, 367–378 (1987).
47. Lee, K. E. et al. Synthesis of kisspeptin-mimicking fragments and investigation of their skin anti-aging effects. *Int. J. Mol. Sci.* **21**, 8439 (2020).
48. Zhao, Y. et al. Rhfgf21 protects epidermal cells against uvb-induced apoptosis through activating ampk-mediated autophagy. *Genes (Basel)*. **23**, 12466 (2022).
49. Ito, S. et al. P62 modulates the intrinsic signaling of uvb-induced apoptosis. *J. Dermatol. Sci.* **83**, 226–233 (2016).
50. Fernando, I. et al. Human keratinocyte uvb-protective effects of a low molecular weight fucoidan from sargassum Horneri purified by step gradient ethanol precipitation. *Antioxid. (Basel)*. **9**, 340 (2020).
51. Huang, S., Shieh, C., Wu, Y., Pan, Y. & Yu, C. Antioxidant activity of spiranthes sinensis and its protective effect against uvb-induced skin fibroblast damage. *Processes* **9**, 1564 (2021).
52. Liu, L. et al. Differential response of normal human epidermal keratinocytes and Hacat cells to hydrogen peroxide-induced oxidative stress. *Clin. Exp. Dermatol.* **37**, 772–780 (2012).
53. Charachit, N., Sukhamwang, A., Dejkriengkraikul, P. & Yodkeeree, S. Hyperoside and Quercitrin in houttuynia cordata extract attenuate uvb-induced human keratinocyte cell damage and oxidative stress via modulation of Mapks and Akt signaling pathway. *Genes (Basel)*. **11**, 221 (2022).
54. Heo, H. et al. Protective activity and underlying mechanism of ginseng seeds against uvb-induced damage in human fibroblasts. *Antioxid. (Basel)*. **10**, 403 (2021).
55. Lee, H., Sung, J., Kim, Y., Jeong, H. S. & Lee, J. Protective effects of unsaponifiable matter from Perilla seed meal on uvb-induced damages and the underlying mechanisms in human skin fibroblasts. *Antioxid. (Basel)*. **8**, 644 (2019).

Acknowledgements

We thank the Key Laboratory of Pathological Biology of Ministry of Education in Jilin University for technical support.

Author contributions

Han Bao: Conceptualization, Investigation, Writing - original draft, Writing - review & editing. Ming Zhu: Visualization, Writing - review & editing. Yizhuo Xie: Visualization, Writing - review & editing. Na Yang: Methodology, Writing - review & editing. Shanshan Wang: Formal analysis. Kejia Chen: Data curation, Validation. Hongzhu Chen: Methodology. Jingwen Dai: Software. Zhiping Li: Visualization, Writing - review & editing. Liangping Yu: Conceptualization, Funding acquisition, Methodology, Project administration, Supervision, Writing - review & editing. Jin Pei: Conceptualization, Funding acquisition, Methodology, Project administration, Resources, Supervision, Writing - review & editing.

Funding

This work was supported by the Science and Technology Development Project from Jilin Science and Technology Department [grant number 20210204067YY].

Declarations

Competing interests

The authors declare no competing interests.

Ethics approval

All operation procedures were in accordance with the China National Institute's Guidelines on the Care and Use of Laboratory. The protocols of animal study (Approval No. 20210072) received approval from the

Ethics Committee of the School of Pharmaceutical Sciences, Jilin University and adhered to the ARRIVE2.0 guidelines.

Additional information

Supplementary Information The online version contains supplementary material available at https://doi.org/10.1038/s41598-025-26409-y.

Correspondence and requests for materials should be addressed to L.Y. or J.P.

Reprints and permissions information is available at www.nature.com/reprints.

Publisher's note Springer Nature remains neutral with regard to jurisdictional claims in published maps and institutional affiliations.